MAPPING RESIDUAL STRESS FIELDS BY ULTRASONIC TOMOGRAPHY

B. P. Hildebrand and D. E. Hufferd
Battelle Northwest
Richland, Washington 99352

ABSTRACT

It is well known that the velocity of sound in a solid is affected by stress. This phenomenon is a third order effect, and has been used primarily as a research tool to determine the Lamé amd Murnaghan elastic constants for various materials. A few preliminary attempts to use it for stress analysis have also been made. In this paper we describe the first attempt to combine this effect with the newly revived mathematical technique known as Computerized Axial Tomography (CAT) to provide quantitative maps of velocity within thick metal sections. From these maps it is possible to infer the state of residual stress within the material. The technique requires that time-of-flight profiles through a section of the solid be made in a number of angular directions. This is equivalent to measuring the velocity through the solid from many different directions in a single plane. The computer takes the set of data so gathered and inverts it to produce a cross-sectional plot of velocity versus position. We have succeeded in mapping velocity anomalies as low as 0.2% and estimate that 0.5% is technically feasible. This kind of sensitivity should allow us to map stress anomalies as low as 1000 psi/inch in steel. We will also describe an experiment with a mild steel section in which we inserted an oversized pin by shrink fitting. The reconstruction clearly shows the high compressive stress within the pin, and the tensile stress in the metal surrounding the pin.

Acknowledgement

This work was sponsored by the Electric Power Research Institute, Palo Alto, California.

References

1. B. J. Ratcliffe, "A Review of the Techniques Using Ultrasonic Waves for the Measurement of Stress Within Materials," British Journal of N.D.T., September 1969.

2. E. I. Crecraft, "Ultrasonic Measurement of Stresses," Ultrasonics, Vol. 6, April 1968.

3. N. H. Hsu, "Acoustical Birefringence and the Use of Ultrasonic Waves for Experimental Stress Analysis," Experimental Mechanics, May 1974.

4. R. T. Smith, "Stress-Induced Anisotropy in Solids - The Acousto-Elastic Effect," Ultrasonics, July-September 1963.

5. P. J. Noronha and J. J. Wert, "An Ultrasonic Technique for the Measurement of Residual Stress," J. of Testing and Evaluation, Vol. 3, March 1975.

6. Technical Digest of the Topical Meeting on Image Processing for 2-D and 3-D Reconstruction from Projections, August 1975, sponsored by Opt. Soc. Am.

7. D. S. Clark and W. R. Varney, "Physical Metallurgy for Engineers," C. VanNostrand, Princeton, N.J., 89-91 (1952).

$$\rho_0 V_L^2 = \lambda + 2\mu + \frac{T}{3K_0}\left[\frac{\lambda+\mu}{\mu}(4\lambda + 10\mu + 4m) + \lambda + 2\ell\right]$$

$$\rho_0 V_T^2 = \lambda + 2\mu - \frac{T}{3K_0}\left[\frac{2\lambda}{\mu}(\lambda + 2\mu + m) - 2\ell\right]$$

ρ_0 = DENSITY

V_L = VELOCITY OF LONGITUDINAL WAVES PROPAGATING IN DIRECTION OF STRESS

V_T = VELOCITY OF LONGITUDINAL WAVES PROPAGATING IN DIRECTION TRANSVERSE TO STRESS

λ, μ = SECOND ORDER LAME ELASTIC CONSTANTS

ℓ, m, n = THIRD ORDER MURNAGHEN ELASTIC CONSTANTS

T = UNIAXIAL TENSION

$K_0 = 1/3\,(3\lambda + 2\mu)$ = BULK MODULUS

FOR COMPRESSION, THE SIGN OF T IS REVERSED

Figure 1. Theoretical variation of longitudinal velocity as a function of stress.

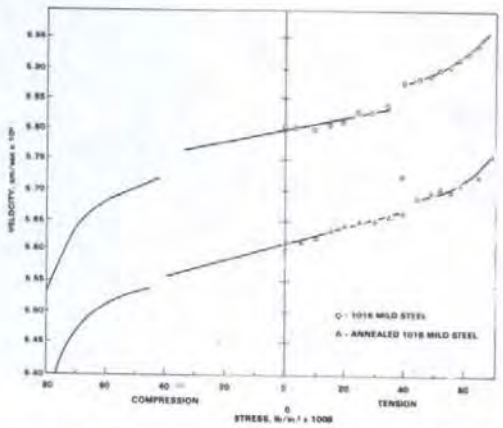

Figure 2. Experimental variation of longitudinal velocity with stress. The annealing was done by heading the sample to 1000°C and cooling at room temperature. Data was taken in tension only. The extrapolation to compression is valid in the linear region, but doubtful beyond the proportional limit.

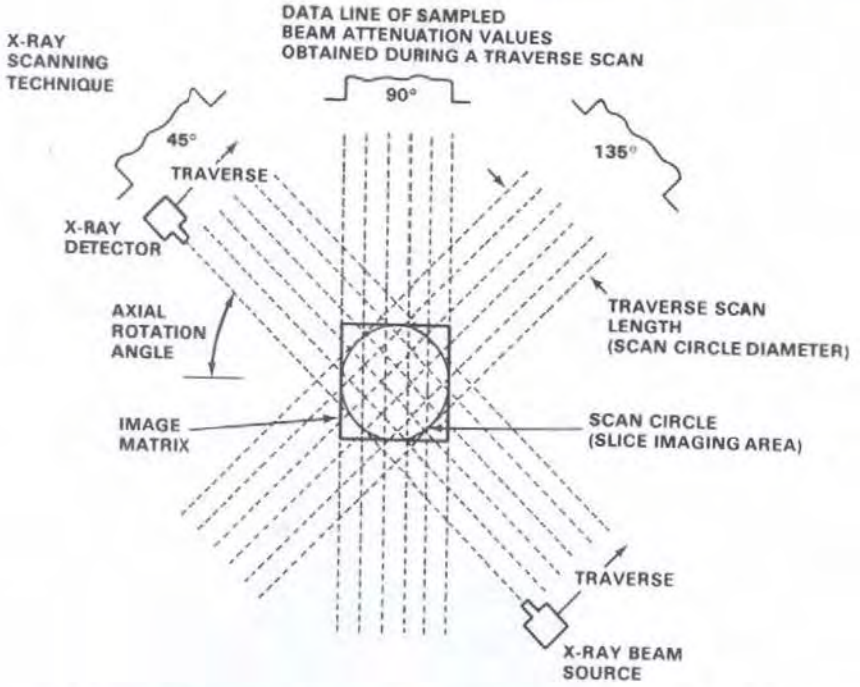

Figure 3. Principle of x-ray tomography. The source and receiver are on opposite sides of a moving frame. Each traverse produces a single projection at a single angle until 180 projections are collected.

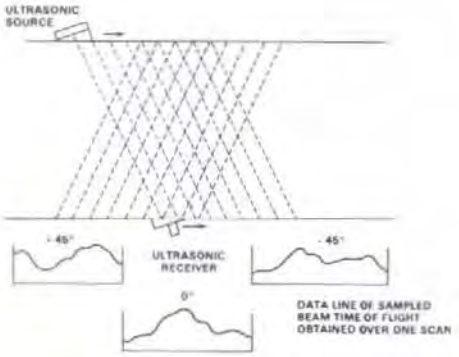

Figure 4. Principle of ultrasonic tomography for thick steel sections. Maximum practical field of view is 90°. This arrangement could be used if both sides of the section are accessible. The reconstruction will yield a cross-sectional plot of the ultrasonic velocity variations.

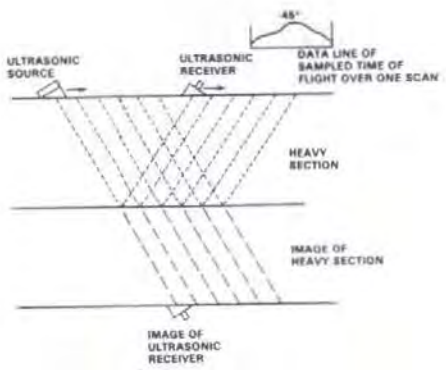

Figure 5. This arrangement could be used if only one side is accessible and the opposite side is smooth. Other angles would be obtained by changing the spacing between source and receiver. The reconstruction would then yield the object and its mirror image.

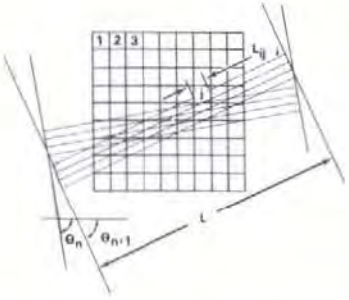

RECONSTRUCTION OF X-RAY TOMOGRAM

$$A_i = \sum_{j=1}^{K} \alpha_j L_{ij} + \alpha_0 \left(L - \sum_{j=1}^{K} L_{ij} \right)$$

WHERE A_i = ATTENUATION ALONG i^{th} RAY (MEASURED)

α_j = ATTENUATION COEFFICIENT IN j^{th} CELL (UNKNOWN)

α_0 = ATTENUATION COEFFICIENT SURROUNDING MEDIUM (KNOWN)

L_{ij} = PATHLENGTH OF i^{th} RAY THROUGH j^{th} CELL (KNOWN)

L = TOTAL PATHLENGTH (KNOWN)

RECONSTRUCTION OF ULTRASONIC TOMOGRAM

$$T_i = \sum_{j=1}^{K} \frac{L_{ij}}{V_j} = \frac{1}{V_w} \left(L - \sum_{j=1}^{K} L_{ij} \right)$$

WHERE T_i = TIME OF FLIGHT ALONG i^{th} RAY (MEASURED)

V_j = VELOCITY IN j^{th} CELL (UNKNOWN)

V_w = VELOCITY IN SURROUNDING MEDIUM (KNOWN)

HENCE, WE HAVE P = NM EQUATIONS WHERE N = TOTAL NUMBER OF RAYS AND M = NUMBER OF ANGLES, AND K UNKNOWNS α_j or V_j. IF K = NM WE CAN SOLVE FOR THE UNKNOWN ATTENUATION OR VELOCITY COEFFICIENTS.

Figure 6. Reconstruction of x-ray and ultrasonic tomogram.

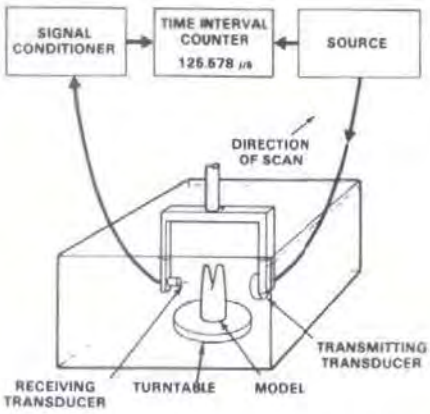

Figure 7. Experimental arrangement for obtaining time-of-flight profiles by through transmission. After each linear scan the model was rotated by 5°. A total of 19 scans were made for a total field of view of 90°. Time-of-flight measurements were made at 21 positions along the scan. Thus a total of 399 measurements were taken, and used to reconstruct 81 points yielding a system of equations having four-fold redundancy.

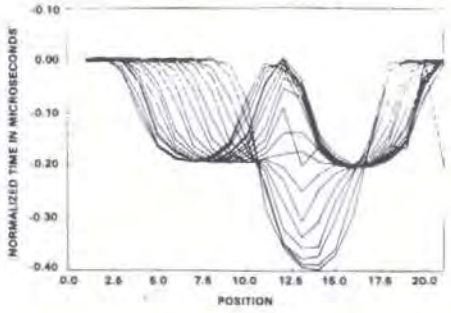

Figure 8. Plots of the time-of-flight profiles taken through the two-fingered glove model. Zero time-of-flight corresponds to the water path and negative times correspond to s-orter flight times. Minimum time occurs when the two fingers lie one behind the other resulting in maximum path through the faster liquid.

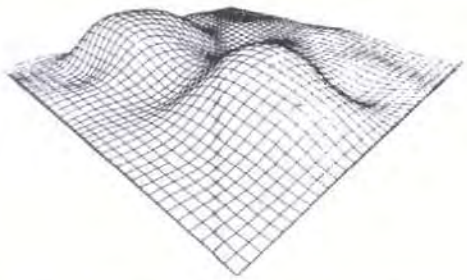

Figure 9. Reconstruction of velocity variation through the two-fingered glove model filled with a liquid whose velocity is 2% higher than that of the surrounding water. The reconstruction was done on a 9 x 9 grid and interpolated to a 40 x 40 grid.

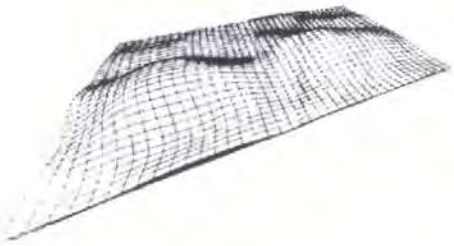

Figure 10. Reconstruction of velocity variation through the two-fingered glove model filled with a liquid who's velocity is 0.2% higher than that of the surrounding liquid.

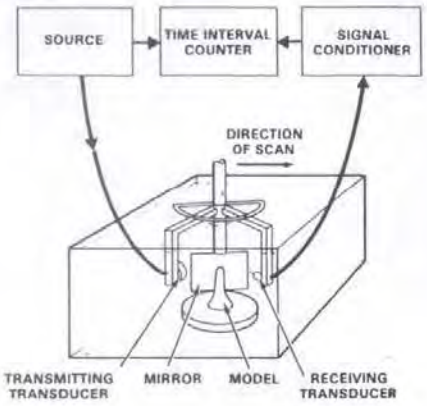

Figure 11. Experimental arrangement for obtaining time-of-flight profiles by reflection. After each linear scan the radial arms of the transducer holders were rotated 2.5^{o} towards each other for a combined change of 5^{o}. A total of 19 scans were made for a total field of view of 90^{o}.

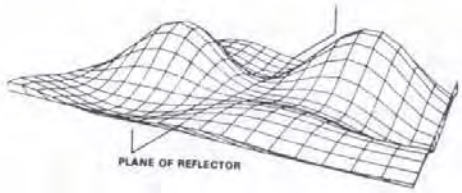

Figure 12. Reconstruction of velocity variation through the one-fingered glove model filled with a liquid who's velocity is 2% higher than that of the surrounding water. This reconstruction was done for the case where the data is taken by reflection, resulting in a mirror image.

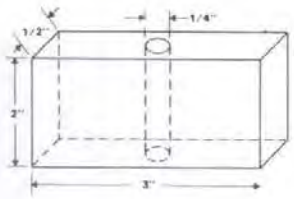

Figure 13. This is a steel model consisting of an oversized pin inserted into a hole. Both were fabricated from the same block of 1018 mild steel. The hole was 0.250 inches in diameter and the pin was 0.252 inches in diameter. The block was heated to $1000^{o}C$, the pin cooled in liquid nitrogen and then forced into the hole. The resulting compressive stress on the pin is estimated to be 108,000 psi.

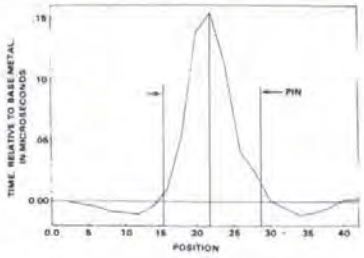

Figure 14. 0^{o} profile through the steel model. Note the increased time-of-flight through the region containing the pin, and the decrease in the regions surrounding the pin.

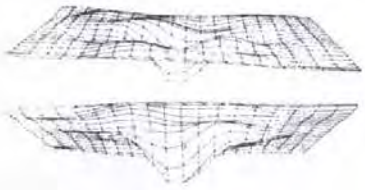

Figure 15. Reconstruction of velocity variations in the steel model. Downward extension represents decreased velocity and, hence, compression. Note that in the surrounding block there is considerable tension stress. From the experimental calibration data we estimate average compressive stress in the pin to be 110,000 psi, maximum tension stress in the block to be 64,000 psi and maximum compression stress in the block to be 90,000 psi.

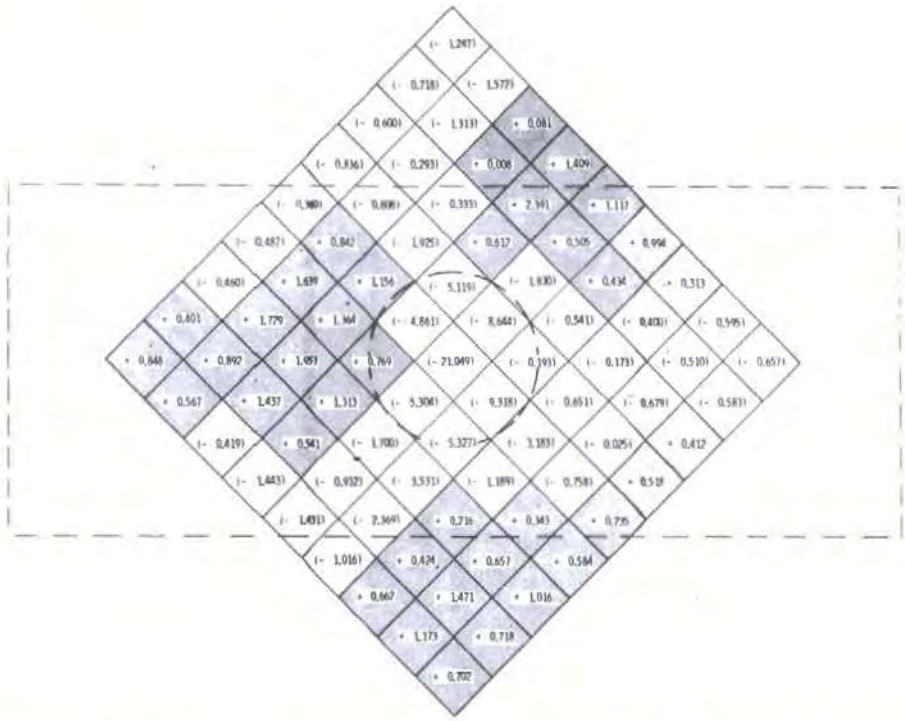

Figure 16. Numerical values for velocity changes in percent related to the geometry of the steel model. Shaded regions indicate velocity increase (tension) and white regions indicate velocity decrease (compression).